On the dynamics of the transition to vortex breakdown in axisymmetric inviscid swirling flows

M. Vanierschot

Abstract

This paper reports on novel features found in the dynamics of the transition to vortex breakdown in inviscid axisymmetric flows with swirl. These features are revealed by a transient simulation of an open ended pipe flow where the inlet swirl is suddenly increased from a swirl number just below the onset of vortex breakdown to a swirl number just above the onset of vortex breakdown. To eliminate the numerous parameters influencing breakdown, the axisymmetric Euler equations with swirl are used as a fluid flow model and solutions are obtained by means of numerical simulation. It is shown that as the step response has died out, the flow evolves to a quasi-static state where time derivatives of variables are negligible small. Stability analysis of this state shows that it can support standing waves in a small region of the flow domain. These standing waves are observed in the

simulations as an imbalance in the axial momentum equation which slows down the flow near the central axis. The amplitude of this imbalance grows exponentially in time with a dimensionless growth rate of 0.83 scaled with the flowthrough time. Eventually, the axial velocity along the central axis becomes negative in a small part of the flow, leading to an axisymmetric recirculation zone, called vortex breakdown. To the authors knowledge, this study would be the first to reveal these features prior to breakdown and the results may help in understanding of the physical mechanisms leading to it as this is still a controversial issue in literature.

1 Introduction

Vortex breakdown has fascinated the scientific community for almost six decades now. It has firstly been discovered by [16] as the bursting of a leading-edge vortex in the flow over a delta wing. Later it has also been found in numerous other engineering flow cases, amongst others rotating pipe flow, jet flow and enclosed cylinder flow. Despite research for over six decades now, there is still no general explanation for vortex breakdown as it is a complex function of numerous flow parameters. Two main general theories exist: the instability theory of [12] and the transition from a supercritical to a subcritical flow by [1]. Ludwieg stated that vortex breakdown is a consequence of hydrodynamic instabilities in the flow which grow in time and eventually lead to breakdown [12]. Benjamin stated that breakdown is

the transition of a supercritical flow (unable to support standing waves) to a subcritical flow (able to support standing waves), similar to the hydraulic jump [1]. As both theories are unable to predict all the features of breakdown found in experiments and simulations, both have found no general acceptance in literature as the main mechanism leading to breakdown.

The main reason for the lack of a general theory is the fact that vortex breakdown manifests itself in many forms which are depend upon many parameters. In experimental work, no less than 7 types have been identified. The two most commonly observed, called bubble and spiral breakdown, were first reported by [9]. Bubble or spiral breakdown have been observed in different experiments with similar settings and even transitions between them within the same experiment (without changing the inflow parameters) have been reported. This has led to disagreement on the origin of breakdown (see for instance the review papers of [5] and [11]). Recent studies showed some more insight in the mechanism leading to breakdown. It was found that flows going from below to above the critical state become unstable [6, 21, 22]. Moreover, it has been shown by numerous authors that spiral breakdown occurs in the wake of an axisymmetric breakdown as a global instability mode of the flow [10, 18, 7, 14, 17, 13, 15]. Two modes of spiral breakdown have been observed: the single helix ($|m|$=1) and the double helix ($|m|$=2), where m is the azimuthal wave number. A recent study of [14] showed that both single or double helix breakdown are a bifurcation from axisymmetric breakdown and that mode selection depends on the swirl number.

In helping to understand the physical phenomena leading to breakdown, this paper studies the dynamics of an axisymmetric inviscid flow just before the onset of vortex breakdown. Analysis of the axial and radial momentum balances and a stability analysis reveals the mechanisms leading to the formation of an axisymmetric breakdown bubble. As such, the results of this study may contribute to more understanding of the physical mechanisms leading to vortex breakdown.

2 Governing equations and boundary conditions

2.1 Pipe geometry

The geometry used in this study is based on the numerical study of [4] and the experimental work of [19] and is also similar to the one used in [2]. A schematic view is shown in figure 1. The geometry is rotational symmetric in the θ direction in a cylindrical (r,θ,z)-coordinate system, where r is the radial, θ the azimuthal and z the axial direction. The pipe is divided into four different sections and the radius of the pipe R(z) as a function of the axial direction z is given as

$$R(z) = \begin{cases} R_i + (R_t - R_i)g(z, z_t), & (0 < z < z_t) \\ R_t + (R_o - R_t)g(z - z_t, z_o - z_t), & (z_t < z < z_o) \\ R_o, & (z_o < z < z_c) \\ \\ R_c + (R_{max} - R_o)g(z - z_c, z_{max} - z_c), & (z_c < z < z_{max}) \end{cases} \tag{1}$$

where the function $g(z, L)$ is defined as

$$g(z, L) = \frac{1}{2}\{1 - \cos[\pi(z/L)]\} \tag{2}$$

and the values of the dimensions are given in table 1. The first section $(0 < z < z_t)$ is convergent which ensures a supercritical flow at z_t to prevent disturbances from traveling upstream towards the inlet section, i.e. it separates the inlet from the vortex breakdown region. The second section $(z_t < z < z_o)$ is diverging to create an adverse pressure gradient on the flow. Adverse pressure gradients are known to promote vortex breakdown [19] and hence the location of the bubble lies within or just after this section. The third section $(z_o < z < z_c)$ has a constant radius and the last section $(z_c < z < z_{max})$ is convergent. This promotes a transition of the flow towards the supercritical state again and hence preventing the output boundary conditions from disturbing the bubble formation.

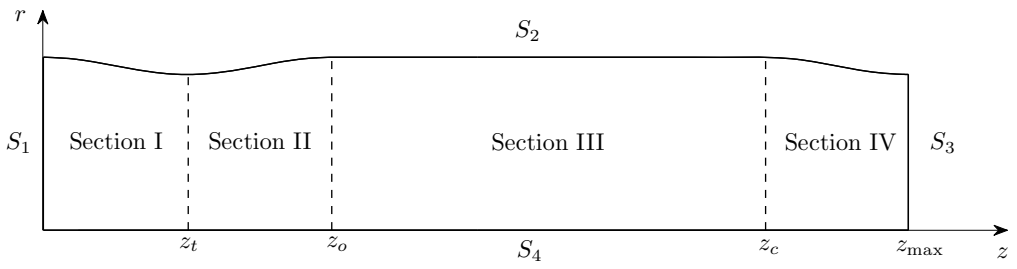

Figure 1: Schematic view of the pipe geometry and the different sections. The radial direction is enlarged by a factor 3 for clarity. The radii in Table 1 corresponding to the axial locations z in the figure have the same index.

Table 1: Values of the pipe geometry constants

z_i	z_t	z_o	z_c	z_{max}	R_i	R_t	R_o	R_c	R_{max}
0	5	10	25	30	2.0	1.8	2.0	2.0	1.8

2.2 Governing equations

Despite the fact that most swirling flows are highly three-dimensional, breakdown often starts axisymmetric, especially for low Reynolds number flows. After the onset of axisymmetric breakdown, helical instabilities start to develop, creating a three-dimensional flow field (e.g. [18]). As this study focuses on the features before breakdown, the axisymmetric variant of the equations are taken were derivatives in the rotational direction are taken to be zero ($\partial/\partial\theta = 0$). The governing equations, called the axisymmetric Euler equations with swirl, are given by:

Table 2: Mean relative difference between the 2D simulations and the reference grid of 180000 cells

δu_z	δu_r	δu_θ	δP
0.01%	0.05%	0.04%	0.04%

$$\frac{1}{r}\frac{\partial r u_r}{\partial r} + \frac{\partial u_z}{\partial z} = 0, \tag{3}$$

for continuity and

$$\frac{\partial u_r}{\partial t} + u_r\frac{\partial u_r}{\partial r} - \frac{u_\theta^2}{r} + u_z\frac{\partial u_r}{\partial z} = -\frac{1}{\rho}\frac{\partial p}{\partial r}, \tag{4}$$

$$\frac{\partial u_\theta}{\partial t} + u_r\frac{\partial u_\theta}{\partial r} + \frac{u_r u_\theta}{r} + u_z\frac{\partial u_\theta}{\partial z} = 0, \tag{5}$$

$$\frac{\partial u_z}{\partial t} + u_r\frac{\partial u_z}{\partial r} + u_z\frac{\partial u_z}{\partial z} = -\frac{1}{\rho}\frac{\partial p}{\partial z}, \tag{6}$$

for (r), (θ) and (z)-momentum where u_r, u_θ and u_z are the velocity components in the radial, azimuthal and axial direction.

2.3 Boundary conditions and numerical procedure

The flow at the inlet (boundary S_1 in figure 1) is modeled as a q-vortex. The non-dimensional velocity profiles for the radial u_r, azimuthal u_θ and axial u_z velocity at the inlet are given by

$$u_r(r) = 0, \quad u_\theta(r) = \frac{\Omega\delta}{r}[1 - \exp(-(\mathrm{r}/\delta)^2)] \quad \text{and} \quad u_z(r) = 1 \tag{7}$$

where Ω is the non-dimensional swirl ratio and $\delta = 1$ is the core radius of the vortex. Often, the amount of swirl is expressed by the swirl number S_w, which is the ratio of axial flux of azimuthal momentum and outer radius times the axial flux of axial momentum,

$$S_w = \frac{\int_0^{R_i} u_\theta u_z r^2 dr}{R_i \int_0^{R_i} u_z^2 r dr}. \tag{8}$$

Substitution of the velocity profiles given in equation 7 into equation 9 and integrating between 0 and R_i results in

$$S_w = \frac{\Omega\delta}{R_i^3}\left(R_i^2 + \delta^2\left[\exp(-(R_i/\delta)^2) - 1\right]\right), \tag{9}$$

which gives for the parameters in this study the relation $S_w \approx 0.3773\Omega$. At the side and outlet boundaries (respectively S_2 and S_3 in figure 1), the gradients off all variables in the normal direction of the boundary are taken to be zero and boundary S_4 is modeled as a symmetry axis. The numerical grid consists of 71 cells in the radial and 625 cells in the axial direction, giving a total number of 44 375 cells. The grid size is taken finer near the central axis to resolve the gradients in the vortex core properly.

The equations of motion are solved using the finite volume method. A Monotonic Upstream-Centered Scheme for Conservation Laws (MUSCL) scheme

is used for the spatial dicretisation as proposed by [20]. For the temporal discretisation, a second order implicit scheme is used. Although this scheme is stable for all time steps chosen the maximum Courant number in the domain is kept below 0.5. Iterations are stopped when the residuals in each cell reach machine accuracy. The level of convergence (LCV), i.e. the sum of the absolute values of the residuals in each cell, to reach machine accuracy for each cell can be estimated as

$$\frac{\phi}{N_{inlet}} N_{total} \times 10^{-8}, \tag{10}$$

where ϕ is the flux variable, N_i the number of inlet cells and N_{total} the total number of celss. Given ϕ is the mass flow rate, this corresponds to a LCV $\approx 10^{-4}$.

In order to assess the discretisation errors, the results are compared to the solution on a 2D reference grid of around 180 000 cells. The results of the average relative error of a variable ϕ, defined as $\delta\phi = \overline{|\phi_{2D} - \phi_{ref}|}/\overline{|\phi_{2D}|}$, where the average is taken over all the grid points in the domain, is shown in table 2. The deviation with the reference grid is maximal 0.05% for both pressure and velocities, indicating that the discretisation errors are sufficiently low.

2.4 Stability analysis

In case of axisymmetric steady flow, the momentum equations 4-6 can be written as a single equation for the streamfunction Φ with the aid of the

vorticity equation as

$$\frac{\partial^2\Phi}{\partial r^2} - \frac{1}{r}\frac{\partial\Phi}{\partial r} + \frac{\partial^2\Phi}{\partial z^2} = r^2\frac{dH}{d\Phi} - C\frac{dC}{d\Phi}, \tag{11}$$

where the streamfunction Φ is given by $u_z = r^{-1}\partial\Phi/\partial r$ and $u_r = -r^{-1}\partial\Phi/\partial z$. This equation is called the Bragg-Hawthorne equation and links the streamfunction with the total head $H = p/\rho + (u_r^2 + u_\theta^2 + u_z^2)/2$ and recirculation $C = ru_\theta$. To check whether the flow can support wave perturbations, we decompose the streamfunction into a base flow Ψ and a very small perturbation ($\epsilon << 1$) as

$$\Phi(r, z) = \Psi(r, z) + \epsilon\phi(r)\exp(kz). \tag{12}$$

Substitution of this expression into equation 11, while linearising towards ϵ results in

$$\begin{array}{l} \frac{\partial^2\phi}{\partial r^2} - \frac{1}{r}\frac{\partial\phi}{\partial r} + \\ \left[k^2 + \frac{1}{r^3u_z^2}\frac{\partial\left(ru_\theta^2\right)}{\partial r} - \frac{r}{u_z}\frac{\partial}{\partial r}\left(\frac{1}{r}\frac{\partial u_z}{\partial r} + \frac{u_r}{ru_z}\frac{\partial u_r}{\partial r}\right)\right]\phi = 0. \end{array} \tag{13}$$

This equation can be written as

$$[C]\cdot[\Phi] = k^2\,[\Phi]\,, \tag{14}$$

where the coefficient matrix $[C]$ depends on the discretisation of the derivatives in equation 13. In this study, both a second order central scheme is used

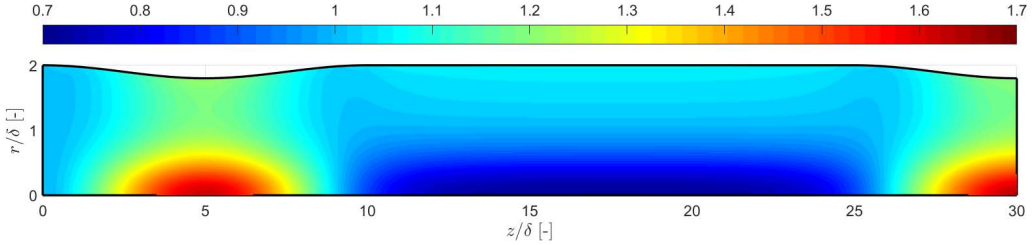

(a) Axial velocity u_z

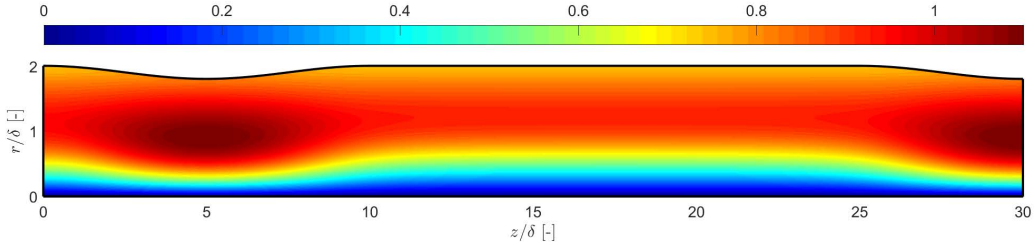

(b) Azimuthal velocity u_θ

Figure 2: Velocity profiles of the 2D simulations for Ω=1.5.

for the first and second order derivatives. The wavenumbers of the perturbation function can be found by solving the eigenvalue problem in equation 14, where k^2 is the eigenvalue. If the eigenvalues are negative, the flow can support standing waves. Note that [1] used a similar equation to check whether a flow is subcritical or supercritical, where in his derivation a columnar vortex is assumed, i.e. u_r =0. In his theory on vortex breakdown, a subcritical flow is able to sustain standing waves (i.e. $k^2 < 0$), while a supercritical flow is unable to support these waves ($k^2 > 0$) and breakdown is then defined as the transition from a supercritical flow to a subcritical flow.

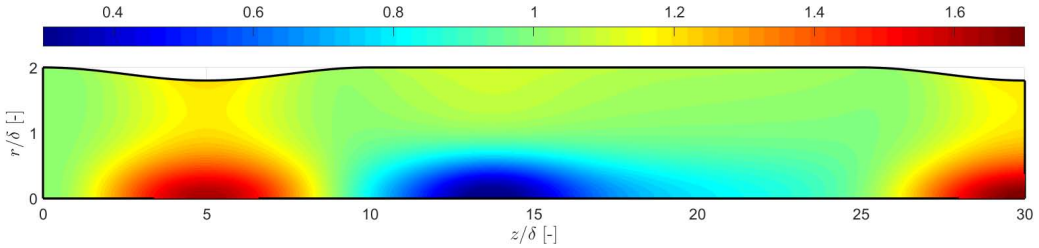

Figure 3: Axial velocity u_z at $t^* = 14/3$ for Ω=1.52.

3 Results and discussion

Simulations with increasing Ω starting from 0 while keeping the profile of u_z constant (results not shown here) show that the transition from a flow without vortex breakdown to a flow with breakdown is somewhere between $\Omega = 1.5$ and 1.52 or $S_w = 0.566$ and 0.573. This critical swirl number is also found by [4] and [2] which performed viscous flow simulations with the same geometry and inlet profiles for Reynolds numbers ranging from $Re = 250$ to 6000. For the higher Reynolds numbers, the transitional swirl number's variation is very small, as confirmed by this study. For $\Omega = 1.5$, the velocity fields of u_z and u_θ are shown in figure 2. As the flow enters the convergent section of the pipe ($0 < z < 5$), it is accelerated and the conservation of azimuthal momentum increases u_θ along the streamlines. In the divergent section of the pipe ($5 < z < 10$), the flow is decelerated by a combination of the positive axial pressure gradients induced by the divergent section of the pipe and the decay of azimuthal velocity. In the constant section of the pipe ($10 < z < 25$), the flow is quite uniform and finally in the convergent section

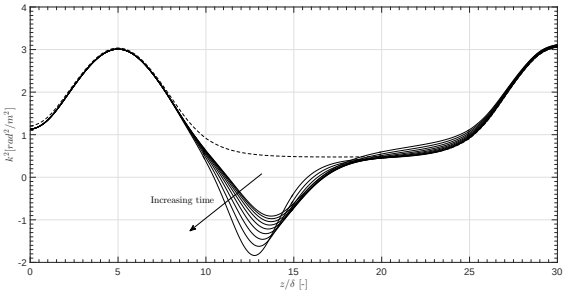

Figure 4: The minimum eigenvalues $|k^2|$ at each axial location. The dashed line corresponds to $\Omega = 1.5$ and the first solid line corresponds to $t^* = 14/3$. The timestep between two adjacent curves is $\Delta t^* = 0.5$, i.e. 0.5 flowthrough times.

of the pipe ($25 < z < 30$) it is accelerated again towards the outlet. The flowfield in figure 2 serves as the initial condition for the transient numerical calculations were a sudden step increase from $\Omega = 1.5$ to 1.52 is simulated. In the following, time t is non-dimensionalised by the flowthrough time as $t^* = t\delta u_z(z = 0)/z_{max}$.

After the sudden increase in inlet swirl, the step response of the flow has died out after around $t^* = 14/3$, i.e. about 5 flowthrough times. The axial velocity field at that timestep is shown in figure 3. This flowfield is called pseudo-static, as the time derivatives of the variables in equations 4-6 are very small compared to the other terms. For instance, considering the axial momentum equation at the central axis,

$$\frac{\partial u_z}{\partial t} = -u_z \frac{\partial u_z}{\partial z} - \frac{1}{\rho}\frac{\partial p}{\partial z}, \tag{15}$$

shows that the maximal time derivative of the velocity, i.e. $\partial u_z/\partial t$ is only

0.01% of the axial momentum-flux $u_z \partial u_z / \partial z$. As the flow field at $t^* \geq 14/3$ is quasi-static, the time derivatives are negligible and solving the eigenvalue problem in equation 13 for each axial location is a good approximation to identify subcritical regions within the flow field and check whether standing waves can exist. The results are shown in figure 4, where the minimum eigenvalue is plotted at each axial location. The dashed line corresponds to $\Omega = 1.5$. At this swirl number, the flow is supercritical in the entire domain and no standing waves are supported. The solid lines corresponds to quasi-static flow fields starting from $t^* = 14/3$ in intervals of $\Delta t^* = 0.5$. The flow at $t^* = 14/3$ is subcritical between $11.2 < z/\delta < 16.6$ and supercritical in the remainder of the domain. Figure 4 shows that the criterion of [1] predicts very well the onset of vortex breakdown if applied locally as also confirmed by other studies, even for viscous flow [18].

Taking the quasi-static flow field at $t^* = 14/3$ as a reference, the perturbation of the radial velocity $\tilde{u}_r(r, z, t^*)$ can be defined as $\tilde{u}_r(r, z, t^*) = u_r(r, z, t^*) - u_r(r, z, t^* = 14/3)$. The time evolution of this perturbation near the central axis (radial location $r/\delta \approx 0.007$) is shown in figure 5. The profile of $\tilde{u}_r$ corresponds to a wave which is located in the part of the domain where the flow is subcritical (see figure 4). The perturbation grows exponentially in time. The dimensionless growth rate of 0.83 is determined by exponential fit of the maximum amplitude in figure 5b versus time. The wavelength of $\tilde{u}_r$ corresponds to $\lambda \approx 2\pi/k_{max}$, where k_{max} is the minimal wavenumber in figure 4. Moreover, this wavelength is also more or less equal to the length

of the region where the flow is subcritical. This close relation between the observed wavelengths and the critical region of the flow supports the theory of Benjamin that vortex breakdown is the transition from supercritical to subcritical flow.

As the perturbations in the flow grow near the central axis, an imbalance is induced between the axial momentum in the flow and the static pressure gradients in the flow direction near the central axis. Figure 5b shows this imbalance as the left hand side of equation 15. The curves in the figure are taken at the same time instants as the ones in figure 4. As the acceleration of the flow is negative just upstream of the critical region, the flow is decelerated along the central axis. Due to this deceleration, the location where the flow becomes subcritical moves upstream, as confirmed by figure 4. As the imbalance grows exponentially in time, the deceleration near the central axis increases, until a region of negative axial velocity is formed, called the vortex breakdown bubble (figure 6). To the authors knowledge, this paper would be the first one to identify this exponential growing imbalance in axial momentum in a region where the flow is subcritical according to Benjamin and this imbalance is the physical mechanism leading to the bubble formation. It is well known in literature that adverse pressure gradients decelerate the flow near the central axis and promote the transition to breakdown, i.e. they decrease the critical swirl number. However, looking at the velocity fields in Figs. 2 and 3 shows that both flows are far from stagnant, i.e. the axial velocity on the centerline is still in the order of 0.3-0.7 m/s. It is

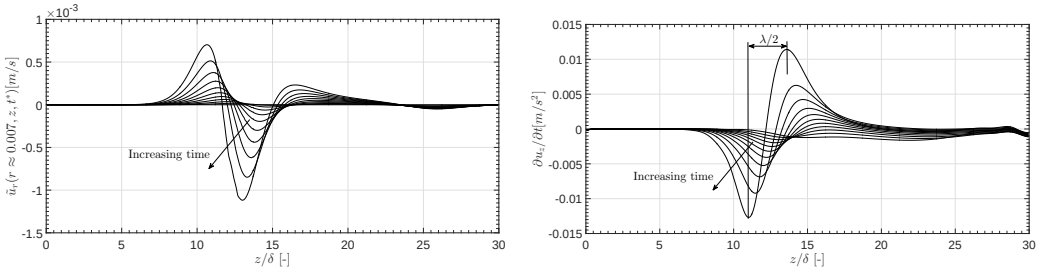

(a) Radial velocity perturbation at $r/\delta \approx 0.007$.

(b) Acceleration of the axial velocity at $r/\delta \approx 0.007$.

Figure 5: Perturbation of radial velocity and momentum imbalance near the central axis at $r/\delta \approx 0.007$. The first line corresponds to $t^* = 14/3$. The timestep between two adjacent curves $\Delta t^* = 0.5$, i.e. 0.5 flowthrough times. The curves are taken at the same time instants as the solid curves in figure 4

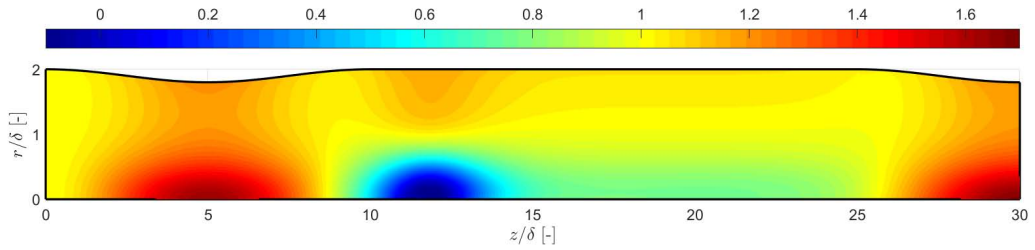

Figure 6: Axial velocity fields at the transition to vortex breakdown. Axial velocity u_z at $t^* = 10$.

also confirmed by [8] that flows near criticality are not necessary flows near stagnation. Therefore, stagnation is a consequence of vortex breakdown and vortex breakdown is not a consequence of stagnation, as also confirmed by [3].

4 Conclusions

This paper studied the dynamics involved in the transition from a swirling flow with swirl number below the onset of vortex breakdown to a swirling flow undergoing breakdown. To eliminate the numerous parameters influencing breakdown, the axisymmetric Euler equations with swirl are used as a fluid flow model and solutions are obtained by means of numerical simulation. It is shown that as the initial swirl increase has died out, the flow evolves to a quasi-static state where time derivatives of variables are very small. Stability analysis of this state shows that it can support standing waves in a small region of the flow domain. As such, this study verifies the criterion of Benjamin, which states that breakdown is the transition from a supercritical flow to a subcritical flow. These standing waves are observed in the simulations as an imbalance in the axial momentum equation which slows down the flow near the central axis. The amplitude of this imbalance grows exponentially in time, eventually leading to an axisymmetric recirculation zone, called vortex breakdown. To the authors knowledge, this study would be the first to reveal these features prior to breakdown and the results may help in understanding of the physical mechanisms leading to breakdown as this is still a controversial issue in literature.

References

[1] T. B. Benjamin. Theory of the vortex breakdown phenomenon. *J. Fluid Mech.*, 14(4):593–629, 1962.

[2] P. S. Beran and F. E. C. Culick. The role of non-uniqueness in the development of vortex breakdown. *J. Fluid Mech.*, 242:491–527, 1992.

[3] A. W. Cary and D. L. Darmofal. Axisymmetric and non-axisymmetric initiation of vortex breakdown. Technical report, RTO AVT Symposium on 'Advanced Flow Management: Part A - Vortex Flows and High Angle of Attack for Military Vehicles', 2001.

[4] D. L. Darmofal and E. M. Murman. On the trapped wave nature of axisymmetric vortex breakdown. *AIAA Paper 94-2318*, 1994.

[5] M. P. Escudier. Vortex breakdown: observations and explanations. *Prog. Aerospace Sci.*, 25:189–229, 1988.

[6] F. Gallaire and J.-M. Chomaz. The role of boundary conditions in a simple model of incipient vortex breakdown. *Phys. Fluids*, 16:274–286, 2004.

[7] F. Gallaire, M. Ruith, E. Meiburg, J.-M. Chomaz, and P. Huerre. Spiral vortex breakdown as a global mode. *J. Fluid Mech.*, 549:71–80, 2006.

[8] M. G. Hall. Vortex breakdown. *Annual Review of Fluid Mechanics*, 4:195–217, 1972.

[9] N. C. Lambourne and D. W. Bryer. The bursting of leading-edge vortices: some observations and discussion of the phenomenon. Technical Report 3282, Ministry of Aviation, Aeronautical Research Council, 1961.

[10] H. Liang and T. Maxworthy. An experimental investigation of swirling jets. *J. Fluid Mech.*, 525:115–159, 2005.

[11] O. Lucca-Negro and T. O'Doherty. Vortex breakdown: a review. *Prog. Energy Combust. Sci.*, 27:431–481, 2001.

[12] H. Ludwieg. Stabilitat der stromung in einem zylindrischen ringraum. *Z. Flugwiss.*, 8(12):135–140, 1960.

[13] T. Luginsland, F. Gallaire, and L. Kleiser. Impact of rotating and fixed nozzles on vortex breakdown in compressible swirling jet flows. *Eur J Mech B-Fluids*, 57:214–230, 2016.

[14] P. Meliga, F. Gallaire, and J.-M. Chomaz. A weakly nonlinear mechanism for mode selection in swirling jets. *J. Fluid Mech.*, 699:216–262, 2012.

[15] K. Oberleithner, M. Sieber, C. Nayeri, C. Paschereit, C. Petz, H.-C. Hege, B. Noack, and I. Wygnanski. Three-dimensional coherent structures in a swirling jet undergoing vortex breakdown: stability analysis and emperical mode construction. *J. Fluid Mech.*, 679:383–414, 2011.

[16] D. H. Peckham and S. A. Atkinson. Preliminary results of low speed wind tunnel test on a ghotic wing of aspect ration 1.0. Technical report, British Aeronaut. Res. Council, 1957.

[17] U. Qadri, D. Mistry, and M. Juniper. Structural sensitivity of spiral vortex breakdown. *J. Fluid Mech.*, 720:558–581, 2013.

[18] M. Ruith, P. Chen, E. Meiburg, and T. Maxworthy. Three-dimensional vortex breakdown in swirling jets and wakes. *J. Fluid Mech.*, 486:331–378, 2003.

[19] T. Sarpkaya. Effect of the adverse pressure gradient on vortex breakdown. *AIAA J.*, 12:602–607, 1974.

[20] B. Van Leer. Toward the ultimate concervative difference scheme. iv. a second order sequel to godunov's method. *J. Comput. Phys.*, 32:101–136, 1979.

[21] S. Wang and Z. Rusak. On the stability of an axisymmetric rotating flow in a pipe. *Phys. Fluids*, 8:1007–1016, 1996.

[22] S. Wang and Z. Rusak. The dynamics of a swirling flow in a pipe and transition to axisymmetric vortex breakdown. *J. Fluid Mech.*, 340:177–223, 1997.